Thermal intensification of microbial Fe(II)/Fe(III) redox cycling in a pristine shallow sand aquifer on the Canadian Shield

V.L. Shirokova, A.M.L. Enright, C.B. Kennedy, F.G. Ferris[*]

Department of Earth Sciences, University of Toronto, 22 Russell Street, M5S 3B1, Toronto, Ontario, Canada

ABSTRACT

This investigation evaluates spatial relationships between summer (July) groundwater temperatures and Fe(II)/Fe(III) biogeochemical cycling over a five year period in a shallow pristine sand aquifer at Meilleurs Bay near Deep River, Ontario, Canada. A warm subsurface thermal island of 12.5−16.1 °C, compared to background conditions of 10−11 °C, was manifest in contour maps of average groundwater temperature over the study period. The warm zone coincided with an area of convergent groundwater flow, implicating horizontal heat transfer by advective convection as the reason for elevated temperatures. Additionally, high concentrations of dissolved Fe(II) and Fe(III) overlapped the warm thermal island, indicative of increased rates of bacterial Fe(II)-oxidation and Fe(III)-reduction. A depletion in the modal abundance of Fe(II)-bearing minerals, notably amphibole and biotite, inside the area of the warm thermal island was also observed, suggesting enhanced mineral dissolution owing to chemoautotrophic Fe(II)-oxidation coupled to the reduction and fixation of dissolved inorganic carbon as biomass. Throughout the aquifer, redox conditions were poised in terms of Eh and pH close to equilibrium with respect to the Fe(II)/Fe(OH)$_3$ couple, feasibly enabling simultaneous bacterial Fe(II)-oxidation and Fe(III)-reduction with an adequate supply of electron acceptors and donors, respectively. The significance of higher groundwater temperature as a determinant of elevated dissolved Fe(II) and Fe(III) concentrations induced by thermal intensification of microbial biogeochemical activities yielded Pearson product-moment correlations in which temperature alone, as a single independent variable, explains almost 30 to nearly 60 percent of the variation in the measured dissolved Fe(II) and Fe(III) concentrations in the groundwater. These results emphasize the important influence of thermal conditions on biogeochemical processes in aquifers coupled to the development of steep gradients in groundwater quality over short distances in shallow unconfined groundwater systems.

1. Introduction

The importance of groundwater systems as the most critical reservoir of freshwater storage on Earth cannot be understated (Taylor et al., 2013; Gleeson et al., 2015). On a global scale, groundwater is estimated to provide 36% of potable drinking water, 42% of irrigation water for agriculture, and 24% of direct-use industrial water; collectively, these groundwater withdrawals are estimated to be on the order of 900 km^3 per year (Foster et al., 2013). Most extractions are taken from recently recharged groundwater sources less than 50 years old, which are considered to be the most sensitive and vulnerable to anthropogenic contamination and climate change (Gleeson et al., 2015; Taylor et al., 2013). Of particular concern is the prospect of global warming and increasing air temperatures bringing about warming in the shallow subsurface thereby affecting biogeochemical processes and, consequently, groundwater quality (Taylor and Stefan, 2009; Kurylyk et al., 2014; Menberg et al., 2014).

The acquisition of solutes and geochemical evolution of groundwater is determined foremost by the weathering rates of minerals along subsurface flow paths (Wilson, 2004; Glynn and Plummer, 2005). The kinetics of these reactions and their impact on groundwater quality are subject not only to acceleration by increasing temperature, but also a wide assortment of physical, chemical, and biological influences (Kump et al., 2000). Reduction-oxidation (redox) transformations are especially important as they are essential for bacterial energy metabolism and biogeochemical cycling, as well as the mobilization or immobilization of potentially

toxic chemical species and degradation of anthropogenic contaminants (Groffman and Crossey, 1999; Chapelle et al., 2009; Barnes et al., 2011; Kumar and Riyazuddin, 2012; Lin et al., 2012; Parsons et al., 2013). Typically, solute concentrations and pH increase in response to longer periods of mineral weathering as redox conditions shift from oxidized recharge zones to more reducing conditions with increasing distance along groundwater flow paths (Kump et al., 2000; Wilson, 2004; Glynn and Plummer, 2005; McMahon and Chapelle, 2008). Although this type of behavior is especially pronounced in regional groundwater systems where residence times are long, local unconfined aquifers are susceptible to redox transitions over much shorter distances (<1.0 km) arising from upland recharge and discharge in adjacent topographic lows (Mitchell and Branfireun, 2005; Ulanowski and Branfireun, 2013).

The complex landscape of the Canadian Shield occupies nearly one-third of the North American landmass (Shilts et al., 1987). Shallow unconfined groundwater systems consisting of glacio-fluvial sands derived from reworked glacial sediments are important hydrogeological remnants left behind on the Canadian Shield in the aftermath of the Wisconsin glaciation and retreat of the Laurentide ice sheet (Catto et al., 1982; Singer and Cheng, 2002; Eyles, 2006). In some areas where their saturated thickness is adequate, the sand units constitute productive local aquifers that are used primarily for drinking-water supply (Montcoudiol et al., 2015). On a regional scale, they interact hydraulically with underlying bedrock aquifers, as well as neighbouring peatlands, wetlands, and lakes (Mitchell and Branfireun, 2005; Ulanowski and Branfireun, 2013; Richard et al., 2014). Hydrogeochemical surveys further indicate that groundwater in these shallow sand aquifers typically resembles recently infiltrated meteoric water with a chemical signature associated with relatively short subsurface residence times (Montcoudiol et al., 2015). Moreover, redox conditions tend to be thermodynamically poised by the Fe(II)/Fe(III) couple, implying an important biogeochemical role for Fe(II)-oxidizing and Fe(III)-reducing bacteria in Canadian Shield hydrogeochemical processes (Mitchell and Branfireun, 2005; Shirokova and Ferris, 2013; Gault et al., 2011, 2012).

This investigation focuses on spatial relationships between groundwater temperature and Fe(II)/Fe(III) biogeochemical cycling in a shallow pristine Canadian Shield groundwater system (Shirokova and Ferris, 2013). Several studies have considered the biogeochemical impact of groundwater warming on groundwater quality associated with urban heat islands and artificial aquifer thermal storage systems (Bonte et al., 2013a, 2013b; Jesußek et al., 2013; Zhu et al., 2015); however, few have been conducted on the extent to which natural horizontal temperature variations associated with groundwater flow impact biogeochemical processes, particularly with respect to shifts in redox conditions and changing rates of mineral weathering. As such, the main objective of this research is to use measurements of groundwater chemistry and temperature from a high-resolution spatial network of piezometers for physicochemical mapping of thermal impacts on microbial Fe(II)/Fe(III) cycling.

2. Methods

2.1. Site description

The study site is a shallow unconfined pristine aquifer in a small forested catchment at Meilleurs Bay on the south bank of the Ottawa River, approximately 10 km west of Deep River in central Ontario, Canada (46°09′42.8″N 77°37′09.5″W) (Catto et al., 1982). The mean annual temperature in the region averages 4.9 °C, ranging from −10.5 °C in January to 18.4 °C in July (Fu et al., 2014;

Montcoudiol et al., 2015). Bedrock in the region is Precambrian in age, consisting of faulted and fractured monzonitic gneiss that is typical of the Grenville Province of the Canadian Shield (Carr et al., 2000). A variety of unconsolidated sediments, predominantly glacial till and post-glacial fluvial sands, overlie bedrock in the region; in some areas thin layers of clay occur on top of the till (Singer and Cheng, 2002; Richard et al., 2014). At the study site itself, aquifer sands were deposited by the Ottawa River between 6000 and 11,200 years ago when the precursors of the Great Lakes drained through the Mattawa and Ottawa Rivers (Lewis et al., 2008). These sands grade into surface exposures of sandy washed till and coarse gravel.

2.2. Hydrogeology and groundwater geochemistry

The aquifer was instrumented with a network of standpipe piezometers to provide repeatable, spatially consistent, measurements over time. The piezometers were constructed from 2.5 cm outer diameter PVC conduit glued to 15 cm length Solinst Model 601 perforated PVC screens fitted with 60 μm polyethylene mesh inserts. The piezometers were inserted into boreholes hand-augered with 5.0 cm outer diameter stainless steel sand corers (AMS). Samples of aquifer sand were collected during installation for mineral identification and modal abundance determinations using X-ray diffraction and petrographic thin-sections (Klein and Philpotts, 2013), and for grain size analyses by sieving to estimate porosity and hydraulic conductivity (Vienken and Dietrich, 2011). Measurements of water depth at each piezometer were done using a Solinst 102 M water level meter.

A Solinst 410 peristaltic pump was used to recover groundwater samples for geochemical analysis; sampling at each piezometer was repeated annually in July from 2010 to 2015. Before sampling, piezometers were bailed completely and allowed to recover at least twice to remove standing water and any silt that may have collected in the piezometer. In order to avoid contact with atmospheric oxygen, groundwater was pumped into a closed 1.5 L flow-through sample cell equipped with a YSI 600 QS multi-electrode sonde for measurement of pH, Eh, temperature, conductivity, and dissolved oxygen. Groundwater samples were vacuum filtered immediately after sampling using 0.22 μm-pore-size membrane filters. Concentrations of dissolved total Fe, Fe(II), and dissolved silica were measured upon filtration using a HACH DR/2500 spectrophotometer with FerroVer®, 1,10 phenanthroline, and heteropoly blue reagents (HACH), respectively. Concentrations of Fe(III) were calculated afterwards as the difference between measured total Fe and Fe(II) concentrations.

2.3. Data analyses

In order to assess spatial relationships between aquifer hydrogeology and groundwater geochemistry, a series of contour maps were constructed using Surfer 11 (Golden Software) including water table elevation, temperature, pH, Eh, and dissolved Fe(II) and Fe(III) concentrations, as well as mineral saturation states for hydroxy-green rust and hydrous ferric oxide. Water table elevation contours were used to infer groundwater flow direction with indicator vector lengths proportional to the slope of the water table surface (i.e., hydraulic gradient) at their location. Statistical analyses were done using STATISTICA 6.0 (StatSoft).

Geochemical modeling was carried out using PHREEQC 3.1.4 to determine the relative saturation state of representative Fe(II) and Fe(III) bearing minerals taken to be plausible constituents of aquifer sand; specifically, hydroxy-green rust $Fe_3O_2(OH)_4$, grunerite (amphibole Fe(II) end-member) $Fe_7Si_8O_{22}(OH)_2$, annite (biotite Fe(II) end-member) $KFe_3AlSi_3O_{10}(OH)_2$, and hydrous ferric oxide

Fe(OH)$_3$ (Parkhurst and Appelo, 2013). Thermodynamic data for hydroxy-green rust and grunerite were obtained from the French Geological Survey (BRGM) PHREEQC database. Solution input parameters included measured values of temperature, pH, Eh, and concentrations of dissolved Fe(II) and Fe(III) at each well; equilibrium conditions with respect to quartz SiO$_2$, and muscovite KAl$_3$Si$_3$O$_{10}$(OH)$_2$, were assumed to provide model constraints for dissolved silica, potassium, and aluminum; as informed by hydrogeochemical data for shallow sand aquifers in the region (Montcoudiol et al., 2015).

3. Results

3.1. Groundwater flow and temperature

The arrangement of piezometers in the study area is shown in Fig. 1A along with water table elevations and vectors for the direction of groundwater flow. In general, groundwater flows predominantly from the southeast in a northwesterly direction. Relative groundwater velocity, as shown by the length of the flow vectors, decreases to the north and west with a pronounced area of
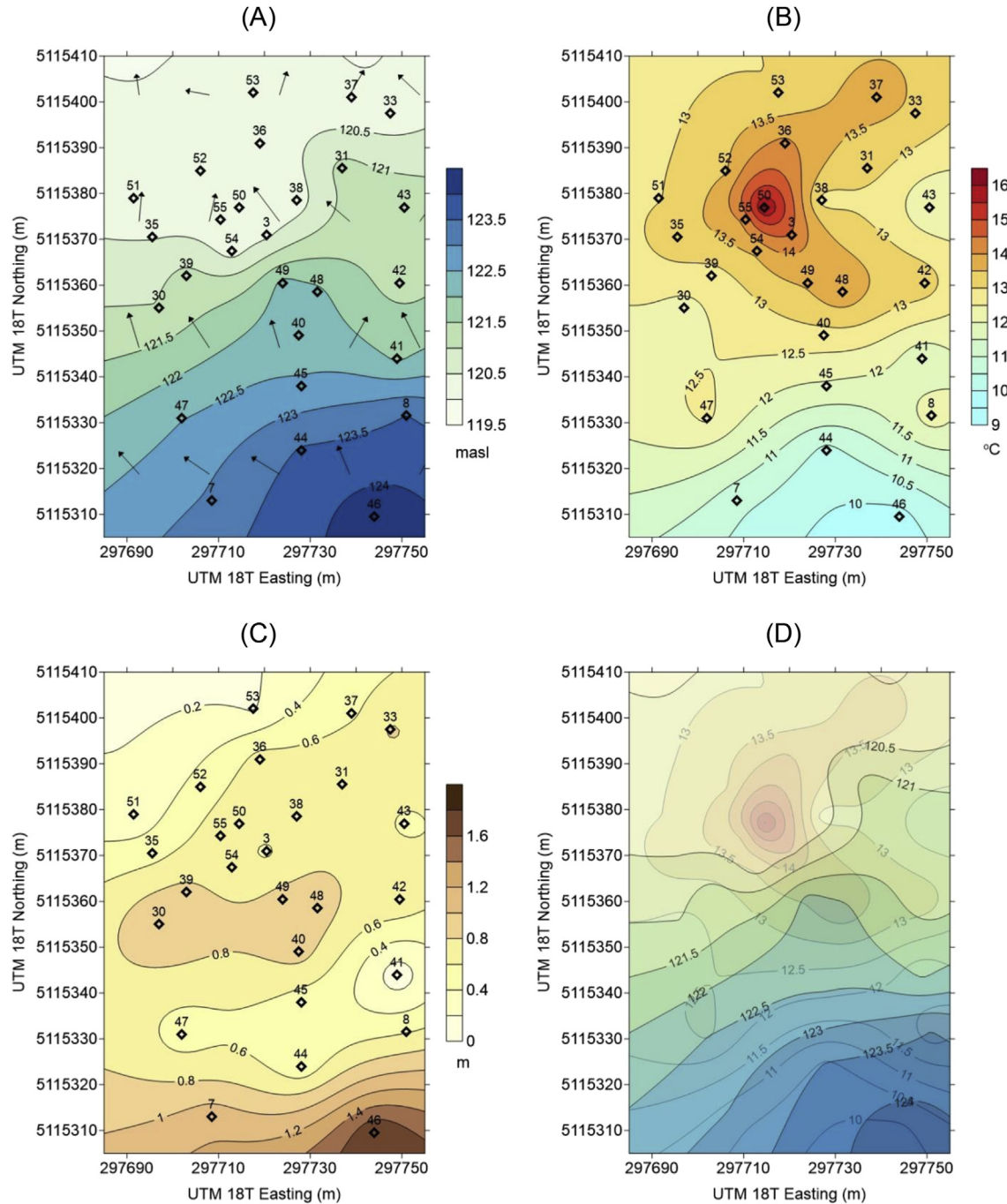

Fig. 1. Contour maps with piezometer locations for (A) the water table elevation and groundwater flow vectors, (B) temperature, and (C) depth to the water table through the unsaturated vadose zone of the Meilleurs Bay aquifer. (D) Overlay of water table elevation and temperature showing the area of the warm groundwater zone at the point of convergent groundwater flow around piezometers 3 and 50.

convergence in flow around piezometers 3, 38, 50, 54 and 55. Grain size analysis yielded a fairly uniform average porosity of 44.0 ± 1.1% throughout the aquifer, with an average hydraulic conductivity of $1.4 \pm 0.3 \times 10^{-4}$ m/s.

The southeast to northwest flow of groundwater is accompanied by a marked increase in average temperature, paralleling a general decrease in vadose zone thickness from almost 2.0 m depth at piezometer 46 to less than 0.2 m at piezometers 41 and 53 (Fig. 1B and C). At the time of groundwater sampling in July, an especially warm thermal island exists in the vicinity of piezometer 50, positioned directly at the point of converging groundwater flow (Fig. 1C and D).

3.2. Aquifer mineralogy

The modal abundances of major mineral constituents comprising the aquifer sand inside and outside the warm thermal island are listed in Table 1. Overall, quartz is the most abundant mineral, followed by plagioclase and biotite, with smaller amounts of muscovite, feldspar, amphibole, and pyroxene. Among these, modal abundances of quartz, muscovite, and feldspar are significantly higher inside the warm zone at $p \leq 0.10$ for the mean difference. In contrast, plagioclase, biotite, and amphibole are depleted in the warm zone; however, the decreases in modal abundance of plagioclase and biotite are only marginally significant at $p = 0.21$ and $p = 0.17$, respectively, compared to a higher degree of significance for the depletion of amphibole ($p = 0.03$). There was no apparent difference in the modal abundance of pyroxene inside or outside of the warm zone. Mineral identities were confirmed by XRD, as well as the presence of trace amounts of 2-line ferrihydrite (i.e., hydrous ferric oxide).

3.3. Geochemistry

Contour maps showing 5 year (2011–2015) average July concentrations for dissolved Fe(II) and Fe(III) are shown in Fig. 2A and B respectively. For both Fe(II) and Fe(III), prominent zones of elevated concentrations are evident immediately around piezometers 3 and 50. In absolute terms, the concentrations of Fe(II) and Fe(III) fluctuated somewhat on a year-to-year basis over the study period (Fig. 2C); however, the high concentration zones remained strictly localized to the same area in the aquifer as the warmest groundwater (compare Fig. 2A and B with Fig. 1B). Measured dissolved silica concentrations in aquifer groundwater were 13.9 ± 0.1 mg/L.

Determination of mineral saturation indices using PHREEQC established that aquifer groundwater, in assumed equilibrium with quartz and muscovite, was orders of magnitude undersaturated (i.e., SI values < −10) with respect to amphibole and biotite Fe(II) end-members grunerite $Fe_7Si_8O_{22}(OH)_2$ and annite $KFe_3AlSi_3O_{10}(OH)_2$, respectively. In contrast, saturation indices for hydrous ferric oxide $Fe(OH)_3$ were all supersaturated ranging from

SI = 0.2 at piezometer 44 to SI = 2.4 at piezometer 3; hydroxy-green rust $Fe_3O_2(OH)_4$ saturation indices ranged from undersaturated SI = −0.35 at piezometer 37 to oversaturated with SI = 4.6 at piezometer 3. Contour plots for greenrust (Fig. 3A) and HFO (Fig. 3B) SI values show that the highest degree of supersaturation occurs in association with the highest groundwater temperatures around piezometers 3 and 50, decreasing gradually towards the northwest in the direction of groundwater flow (Fig. 1).

A plot of average measured Eh and pH values for all of the piezometers in the study area is shown in Fig. 4. Groundwater pH varied over a relatively narrow range, from 5.6 at piezometer 33 to 6.3 at piezometer 52. Eh was lowest at piezometers 3 and 50 where high concentrations of dissolved Fe(II) (>1.0 mg/L), and low concentrations of dissolved oxygen (<3.5 mg/L), were observed. Conversely, piezometers with lower Fe(II) concentrations (<0.05 mg/L) and high dissolved oxygen (>5.0 mg/L), for example 36 and 53, exhibited higher Eh. Collectively, the Eh and pH of all piezometers fall within a band constrained in equilibrium thermodynamic terms by the Nernst equation and Fe(II)/Fe(OH)₃ redox couple with an upper boundary at the minimum Fe(II) concentration of 0.01 mg/L, and lower boundary at the maximum Fe(II) concentration of 1.35 mg/L.

The overall dependence of dissolved Fe(II) and Fe(III) concentrations on pH, Eh, dissolved oxygen concentration, and temperature is quantified in Table 2 by the corresponding Pearson product-moment correlation coefficients. For both Fe(II) and Fe(III), pH and dissolved oxygen concentrations yielded the weakest ($p > 0.05$) negative correlation coefficients, accounting for only 0.5 to 4.3 percent of the variance in the data. Taking natural logarithms into account for the apparent exponential range of Fe(II) and Fe(III) concentrations observed in the aquifer (Fig. 2C) improved the explanation of variance somewhat, notably from 3.0 to 22.2 percent in the case of Fe(III) and pH. Stronger negative correlations were obtained for Fe(II) and Eh, accounting for up to 38.3 percent of the variance, compared to only 18.8 percent of the variance for Fe(III). Temperature was positively correlated with Fe(II) and Fe(III) concentrations, accounting for 29.0 and 20.1 percent of the variance, respectively; this improved to 26.9 and 57.6 percent of the variance for the natural logarithm of the concentrations. Inverse temperature, as informed by the Arrhenius relationship for temperature dependence of reaction rates, yielded expected negative correlations (Langmuir, 1997; Kump et al., 2000), but did not improve the explanation of variance.

4. Discussion

Thermal conditions in near-surface unconfined aquifer systems are strongly influenced by convective heat transport associated with the movement of groundwater, especially at hydraulic conductivities greater than 10^{-7} m/s (Anderson, 2005; Ferguson et al., 2006); this theoretical limit is about 3 orders of magnitude lower

Table 1
A comparison of modal abundances and corresponding differences for minerals in aquifer sand inside (>14 °C) and outside (<12.5 °C) the warm groundwater thermal island. The minerals are listed in order of increasing susceptibility to weathering.

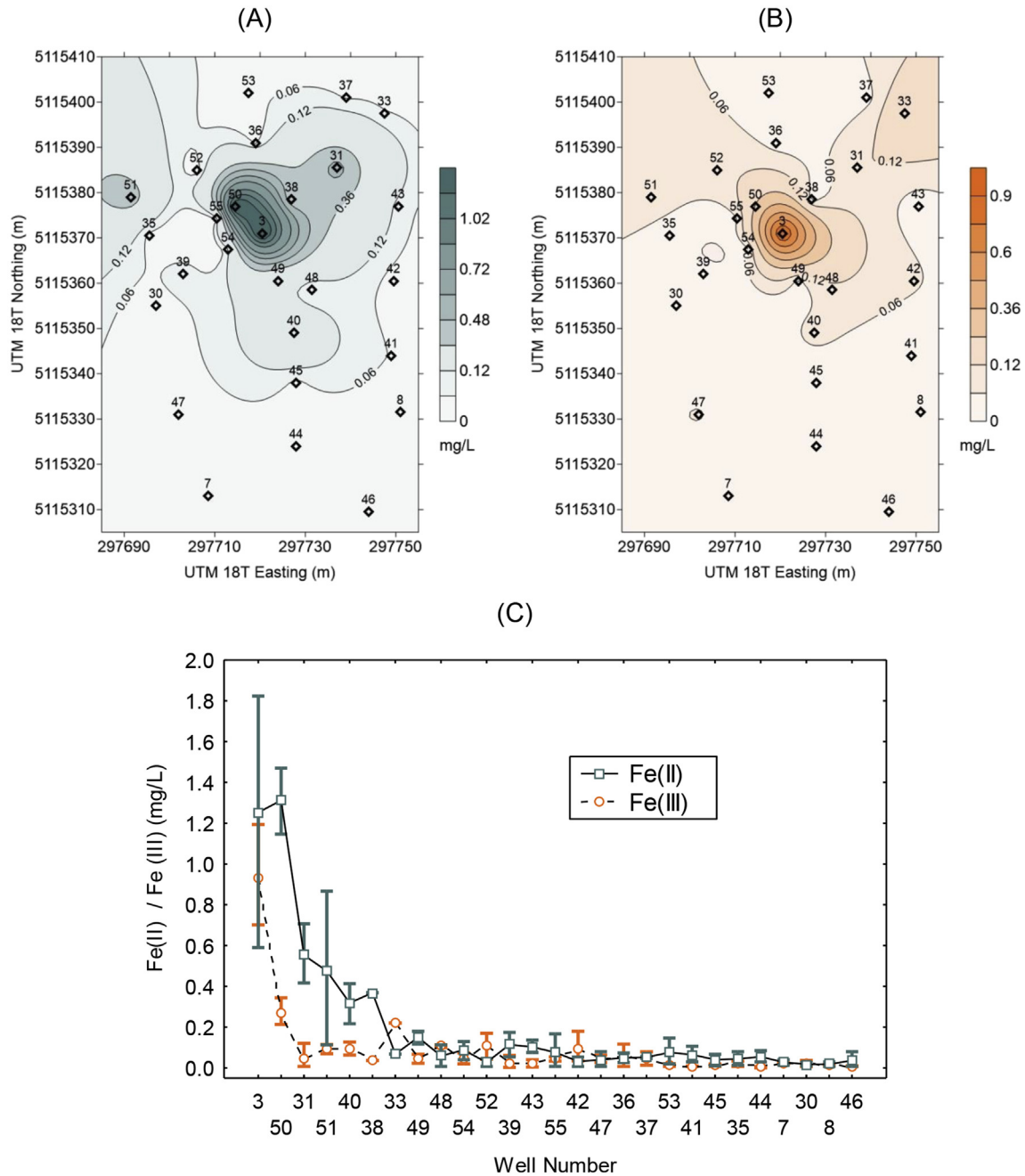| Mineral	Modal abundance % (Mean ± SE)		Difference modal abundance	p value mean difference
	Inside > 14.0 °C (n = 5)	Outside < 12.5 °C (n = 7)		
Quartz	58.5 ± 4.7	52.3 ± 1.4	6.2	0.08
Muscovite	1.8 ± 0.5	1.0 ± 0.4	0.8	0.10
Feldspar	8.3 ± 3.1	4.2 ± 1.4	4.1	0.10
Plagioclase	15.5 ± 3.9	18.5 ± 1.3	−3.0	0.21
Biotite	11.9 ± 1.9	15.0 ± 2.1	−3.1	0.17
Amphibole	1.0 ± 0.1	6.3 ± 2.0	−5.3	0.03
Pyroxene	2.3 ± 1.7	2.3 ± 0.8	0.0	0.50

Fig. 2. Contour maps with piezometer locations for dissolved concentrations of (A) Fe(II) and (B) Fe(III) in the Meilleurs Bay aquifer. (C) Line plots of July averages and corresponding minimum/maximum range of dissolved concentrations of Fe(II) and Fe(III) measured at each piezometer in the Meilleurs Bay aquifer over the 5 year study period; values are displayed in order of decreasing concentrations.

than the hydraulic conductivity determined by grain-size analysis for the Meilleurs Bay aquifer. The effects of convection include density driven pore water flow induced by temperature gradients, as well as flow arising from hydraulic gradients (Anderson, 2005; Bense and Beltrami, 2007; Kurylyk et al., 2014). At the study site, the general south to north trend of increasing groundwater temperature evident in July is consistent with infiltration of warm meteoric water through a progressively thinner vadose zone, along with a slowing in groundwater flow. Further intensification of warming and development of a localized warm thermal island in the aquifer is assumed to arise from focused orientations of groundwater flow, as suggested in other studies on the impact of horizontal convection and heat transfer on the occurrence of

shallow subsurface temperature anomalies (Bense and Beltrami, 2007; Zhu et al., 2015).

The significant differences in modal mineral abundance of aquifer sand inside and outside the warm thermal island follows a classic weathering trend; pyroxene, amphibole, biotite, and plagioclase are recognized as being the most susceptible to weathering, whereas feldspars, muscovite, and quartz are more resistant (Kump et al., 2000; Wilson, 2004). Moreover, increasing temperature accelerates dissolution rates, which accounts for the relative depletion of minerals susceptible to weathering compared to more resistant mineral phases. For example, considering a nominal temperature increase of 5 °C with a 60–80 kJ/mol range of activation energy feasible for mineral dissolution, rates would
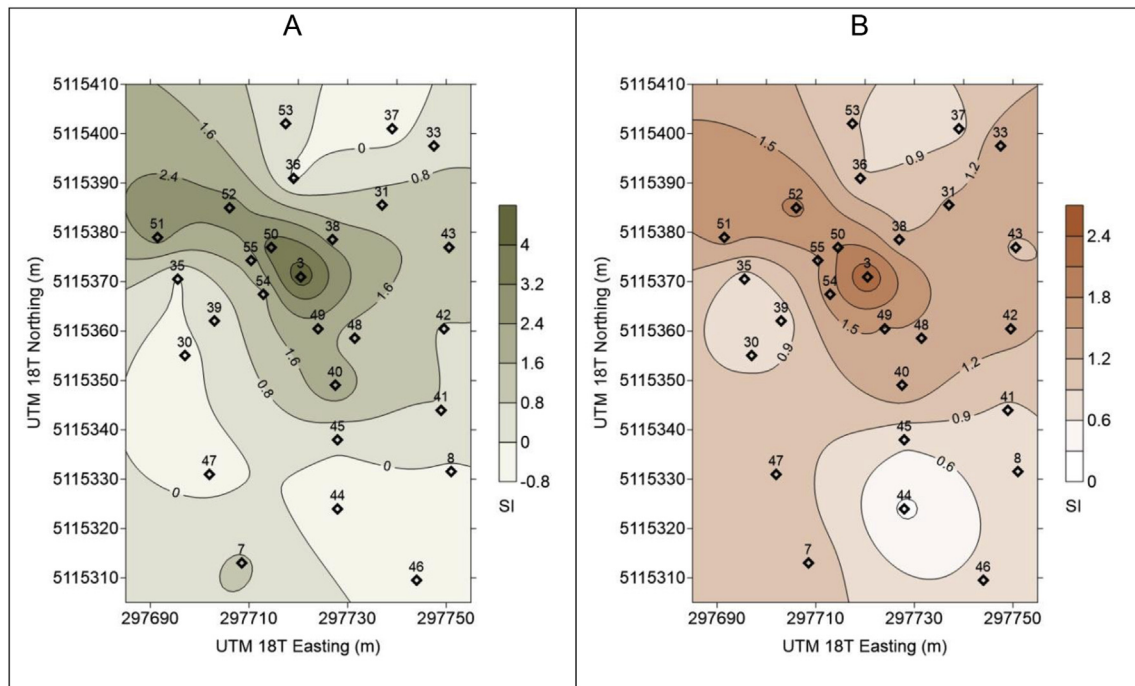
Fig. 3. Contour plots of mineral saturation indices determined using PHREEQC for (A) hydroxy-green rust Fe3O2(OH)4 and (B) hydrous ferric oxide Fe(OH)3 at each piezometer in the Meilleurs Bay aquifer. (For interpretation of the references to colour in this figure legend, the reader is referred to the web version of this article.)
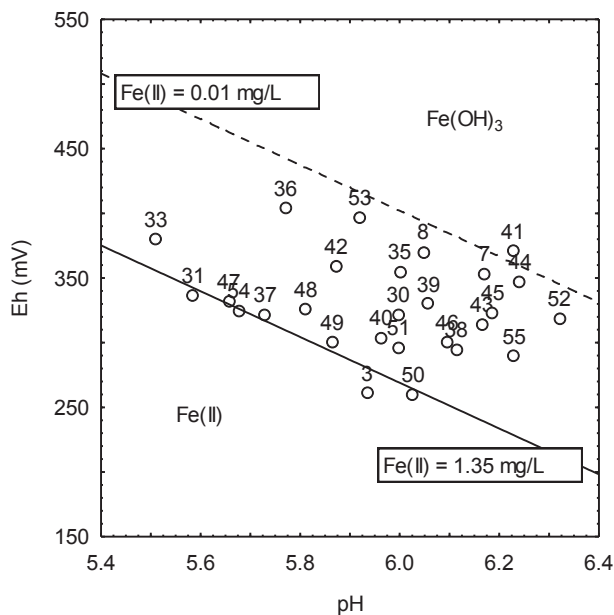

Fig. 4. Scatterplot of average July Eh and pH values at each piezometer in the Meilleurs Bay aquifer; redox boundary lines are shown for the thermodynamic equilibrium Eh and pH calculated using the Nernst equation for the Fe(II)/Fe(OH)3 redox couple with Eh0 = 1065 mV; the dashed upper boundary line is for a Fe(II) concentration of 0.01 mg/L, whereas the solid lower boundary line is for a Fe(II) concentration of 1.35 mg/L.

nearly double based on the Arrhenius relationship (Langmuir, 1997; Kump et al., 2000). Although this investigation provides no insight concerning the seasonal stability of the warm thermal island at the study site, it is reasonable to suppose that many years of elevated temperatures and increased weathering in summer account for the observed pattern of mineral weathering in the aquifer. In terms of

time scale, the longer-term limit for such periodic forcing of temperature accelerated weathering would be no more than 6 to 12 ka, based on estimates for when the aquifer sands were deposited by the Ottawa River, but probably much less owing to changing climate conditions (Catto et al., 1982; Eyles, 2006; Lewis et al., 2008).

The spatial overlap in areas of high dissolved Fe(II) and Fe(III) concentrations with the warm thermal island is a prominent hydrogeochemical feature of the study site. At the same time, the relatively stationary positioning of the zones of high Fe(II)/Fe(III) concentrations implies near steady-state advective reactive solute transport with a tight spatiotemporal coupling between source and sink reactions. Dissolution of Fe(II)-bearing minerals such as amphibole and biotite, as well as bacterial reduction of Fe(III)-oxides, constitute the most plausible sources for Fe(II), whereas chemical and bacterial oxidation of dissolved and solid phase Fe(II) comprise likely sources of Fe(III) (Shebolina et al., 2012; Melton et al., 2014). Precipitation of Fe(III) as HFO, and in conjunction with Fe(II) as green rust, represent probable sinks (Parmar et al., 2001; Berthelin et al., 2006; Vollrath et al., 2012, 2013; Etique et al., 2014; Ferris et al., 2016). Altogether, as a coupled biogeochemical reaction network mediating Fe(II)/Fe(III) redox cycling, these reactions are thermodynamically subject to thermal intensification, which is spatially manifest in the area of the warm thermal island (Jesußek et al., 2013; Bonte et al., 2013a, 2013b).

A previous study evaluating the taxonomic diversity and metabolic capacity of bacteria in the Meilleurs Bay aquifer revealed a diverse microbial community capable of cycling carbon, iron, nitrogen, and sulfur (Shirokova and Ferris, 2013). Operational taxonomic units (OTU) with the capacity to utilize the Fe(II)/Fe(III) redox couple were particularly well represented, including bacterial species capable of using Fe(III) as a terminal electron acceptor for anaerobic respiration and chemoautotrophs that oxidize Fe(II) to generate energy. The strong potential for Fe(II)/Fe(III) cycling between these two metabolic groups of bacteria is emphasized by the observed balance in redox conditions with Eh and pH poised
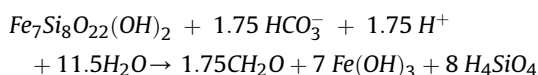
Table 2
Pearson product-moment correlation coefficients (R) and the percentage of explained variance (σ^2) for dissolved Fe(II) and Fe(III) concentrations as functions of pH, redox potential (Eh), dissolved oxygen concentration, temperature (Celsius), and inverse temperature (Kelvin); correlations in bold italic are significant at a level of $p < 0.05$.

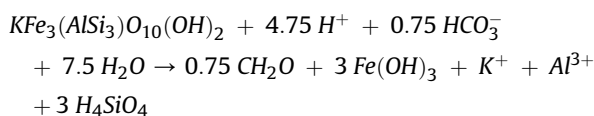| Variable	Fe(II) mg/L		Fe(III) mg/L		ln [Fe(II) mg/L]		ln [Fe(III) mg/L]	
	R	$\%\sigma^2$	R	$\%\sigma^2$	R	$\%\sigma^2$	R	$\%\sigma^2$
pH	−0.07	0.5	−0.17	3.0	−0.16	2.6	***−0.47***	22.2
Eh (mV)	***−0.62***	38.2	−0.43	18.8	***−0.5***	33.3	−0.36	13.3
Dissolved Oxygen (mg/L)	−0.21	4.3	−0.11	1.3	−0.36	13.0	−0.33	11.2
Temperature °C	***0.54***	29.0	***0.45***	20.1	***0.52***	26.9	***0.76***	57.6
1/Temperature °K	***−0.54***	28.7	***−0.45***	19.9	***−0.52***	26.8	***−0.76***	57.6

close to equilibrium with respect to the Fe(II)/Fe(OH)$_3$ redox couple. This means that both Fe(III)-reduction and Fe(II)-oxidation are energetically feasible when adequate supplies of corresponding electron donors and acceptors simultaneously coexist; organic matter in the case of Fe(III)-reduction, and oxygen or nitrate for Fe(II)-oxidation (McMahon and Chapelle, 2008; Chapelle et al., 2009; Bird et al., 2011; Melton et al., 2014; Shen et al., 2015). Similar close associations between Fe(II)-oxidizing and Fe(III)-reducing bacteria has been reported in other aqueous systems, ranging from groundwater discharge zones to estuarine and lake sediments (Roden et al., 2004; Gault et al., 2011, 2012; Lin et al., 2012; Kato et al., 2012).

Despite the high degree of undersaturation with respect grunerite and annite as representatives of Fe(II)-bearing amphibole and biotite minerals, respectively, background groundwater concentrations of dissolved Fe(II) outside the warm thermal island are quite low. The implication is that chemical dissolution rates must be extremely slow in relation to groundwater flow velocities (Kump et al., 2000; Wilson, 2004; Glynn and Plummer, 2005). For this reason, it is difficult to imagine that even a doubling of mineral dissolution rates with increased temperature can account for the observed increase in Fe(II) concentrations. Instead, it is possible that a combination of increased temperature and solid phase chemoautotrophic bacterial Fe(II)-oxidation, with concomitant hydrolysis and precipitation of Fe(III) as HFO, served to increase the elementary mineral dissolution rate, in accordance with Le Chatellier's principle (Langmuir, 1997). With grunerite and annite as examples, the overall reactions are:

Grunerite

$$Fe_7Si_8O_{22}(OH)_2 + 1.75\,HCO_3^- + 1.75\,H^+$$
$$+ 11.5H_2O \rightarrow 1.75CH_2O + 7\,Fe(OH)_3 + 8\,H_4SiO_4$$

Annite

$$KFe_3(AlSi_3)O_{10}(OH)_2 + 4.75\,H^+ + 0.75\,HCO_3^-$$
$$+ 7.5\,H_2O \rightarrow 0.75\,CH_2O + 3\,Fe(OH)_3 + K^+ + Al^{3+}$$
$$+ 3\,H_4SiO_4$$

In these reactions, solid phase Fe(II) is consumed by metabolic oxidation coupled to the reduction of dissolved inorganic carbon as bicarbonate to produce biomass, expressed in general form as CH_2O (Bird et al., 2011; Melton et al., 2014); thereby enhancing mineral dissolution. Support for this kind of reaction sequence comes from laboratory studies documenting the solid phase oxidation of Fe(II) in biotite by chemoautotrophic Fe(II)- oxidizing bacteria (Shelobolina et al., 2012).

The production of Fe(III) and organic matter by Fe(II)-oxdizing bacteria has considerable potential to benefit Fe(II)-reducing bacteria, yielding a prospective source of electron donors and electron acceptors for anaerobic respiration (Chapelle et al., 2009; Shen et al., 2015). This could be especially significant under low nutrient oligotrophic conditions in groundwater systems (Goldscheider et al., 2006). Moreover, there is ample evidence indicating that bacterially produced HFO is more soluble and preferentially reduced by Fe(II)-reducing bacteria in comparison to other more crystalline forms of Fe(III)-oxides, such as goethtite (Bonneville et al., 2004, 2009; Langley et al., 2009; Ferris et al., 2016). In turn, the metabolic production of dissolved Fe(II) by Fe(II)-reducing bacteria would yield an energy source for Fe(III)-oxidizing bacteria, effectively closing the loop on the biogeochemical Fe(II)/Fe(III) redox cycle (Bird et al., 2011; Melton et al., 2014).

A parallel indicator for the local temperature intensification of bacterial Fe(II)-oxidation and Fe(III)-reduction is the increased degree of supersaturation observed for HFO and greenrust in the vicinity of the thermal island. In a thermodynamic biogeochemical context, these two mineral phases represent intermediate metabolic products with the potential to undergo precipitation owing to a state of supersaturation (Parmar et al., 2001; Bonneville et al., 2004, 2005; Berthelin et al., 2006; Vollrath et al., 2012, 2013; Etique et al., 2014; Ferris et al., 2016). If precipitation occurred at a rate fast enough to match corresponding rates of Fe(II)-oxidation and Fe(III)-reduction, the expectation would be for the groundwater to be near equilibrium, rather than supersaturated. This is not the case, suggesting that the rates of HFO and greenrust precipitation are kinetically slow in comparison to bacterial Fe(II)/Fe(III) metabolisms. The implication, in terms of the Arrhenius relationship, is that abiotic HFO and greenrust precipitation rates are not as sensitive to temperature because of lower activation energies in comparison to bacterial Fe(II)/Fe(III) metabolic reactions (Etique et al., 2014; Klueglein and Kappler, 2013; Vollrath et al., 2013). Eventually, saturation states of HFO and green rust decrease, along with dissolved Fe(II) and Fe(III) concentrations, down gradient of the thermal island as expected for solute dispersion arising from groundwater flow.

The overall importance of higher groundwater temperature as a determinant of elevated dissolved Fe(II) and Fe(III) concentrations induced by thermal intensification of microbial biogeochemical activities is tempered somewhat by relatively moderate statistical correlations determined for the aquifer data; however, this does affirm that a multitude of physical, chemical, and biological processes exert a measure of influence on groundwater geochemistry (Glynn and Plummer, 2005; Goldscheider et al., 2006; McMahon and Chapelle, 2008; Ayuso et al., 2009; Barnes et al., 2011; Lin et al., 2012). Even so, this does not diminish the significance of temperature as a critical determinant for Fe(II)/Fe(III) biogeochemical cycling since, as a single independent variable, temperature alone explains almost 30 to nearly 60 percent of the variation in the measured dissolved Fe(II) and Fe(III) concentrations in the groundwater. Exactly how this changes at the study site over the course of a year, from summer to winter, is not presently known and warrants investigation. Certainly, prospects for further

research on how temperature influences biogeochemical processes in shallow subsurface environments are intriguing, especially in view of the growing body of work linking climate change and warming surface temperatures to groundwater warming (Taylor and Stefan, 2009; Menberg et al., 2014; Kurylyk et al., 2014).

5. Conclusion

A warm thermal island exists in the shallow glaciofluvial sand aquifer at Meilleurs Bay, which can be attributed to infiltration of warm meteoric water and a localized area of converging horizontal groundwater flow. Increased temperature in the vicinity of the warm thermal island promotes increased microbial cycling of Fe(II) and Fe(III), thereby accelerating the weathering rates of Fe(II)-bearing amphibole and biotite minerals, as well as contributing to the potential precipitation of secondary minerals such as HFO and greenrust. Understanding how these reactions respond to thermal conditions is important for management of groundwater resources because they are apt to play an important role in regulating the fate and behavior of possibly toxic redox-active chemical species in shallow aquifer systems. Furthermore, the observed meter scale of thermal and biogeochemical spatial heterogeneity over the aquifer emphasizes that it is important to be mindful of possible fluctuations and steep gradients in groundwater quality over short distances in unconfined aquifer systems on the Canadian Shield and elsewhere.

Acknowledgements

References

Anderson, M.P., 2005. Heat as a ground water tracer. Ground Water 43, 951–968.

Ayuso, S.V., Guerrero, M.C., Montes, C., Lopez-Archilla, A.I., 2009. Spatiotemporal distribution of microbial communities in a coastal, sandy aquifer systems (Doñana, SW Spain). Geobiology 7, 66–81.

Barnes, N.A., Kehew, A.E., Krishnamurthy, R.V., Koretsky, C.M., 2011. Redox evolution in glacial drift aquifers: role of diamicton units in reduction of Fe(III). Environ. Earth Sci. 62, 1027–1038.

Bense, V., Beltrami, H., 2007. Impact of horizontal groundwater flow and localized deforestation on the development of shallow temperature anomalies. J. Geophys. Res. 112, F04015.

Berthelin, J., Ona-Nguema, G., Stemmler, S., Quantin, C., Abelmoula, M., Jorand, F., 2006. Bioreduction of ferric species and biogenesis of green rusts in soils. Comptes Rendus Geosci. 339, 447–455.

Bird, L.J., Bonnefoy, V., Newman, D.K., 2011. Bioenergetic challenges of microbial iron metabolisms. Trends Microbiol. 19, 330–340.

Bonneville, S., Van Cappellen, P., Behrends, T., 2004. Microbial reduction of iron(III) oxyhydroxides: effects of mineral solubility and availability. Chem. Geol. 212, 255–268.

Bonneville, S., Behrends, T., Van Cappellen, P., 2009. Solubility and dissimilatory reduction kinetics of iron(III) oxyhydroxides: a linear free energy relationship. Geochim. Cosmochim. Acta 73, 5273–5282.

Bonte, M., Röling, W.F.M., Zaura, E., van der Wielen, P.W.J.J., Stuyfzand, P.J., van Breukelen, B.M., 2013a. Impacts on shallow geothermal energy production on redox processes and microbial communities. Environ. Sci. Technol. 14, 14476–14484.

Bonte, M., van Breukelen, B.M., Stuyfzand, P.J., 2013b. Temperature-induced impacts on groundwater quality and arsenic mobility in anoxic aquifer sediments used for both drinking water and shallow geothermal energy production. Water Res. 47, 5088–5100.

Carr, S.D., Easton, R.M., Jamieson, R.A., Culshaw, N.G., 2000. Geologic transect across the Grenville orogeny of Ontario and New York. Can. J. Earth Sci. 37, 193–216.

Catto, N.R., Patterson, R.J., Gorman, W.A., 1982. The late quaternary geology of the Chalk river region, Ontario and quebec. Can. J. Earth Sci. 19 (6), 1218–1231.

Chapelle, F.H., Bradley, P.M., Thomas, M.A., McMahon, P.B., 2009. Distinguishing iron-reducing from sulfate-reducing conditions. Ground Water 47, 300–305.

Etique, M., Jorand, F.P., Zegeye, A., Gregoire, B., Depas, C., Ruby, C., 2014. Abiotic process for Fe(II) oxidation and green rust mineralization driven by a heterotrophic nitrate reducing bacteria (Klebsiella mobilis). Environ. Sci. Technol. 48, 3742–3751.

Eyles, N., 2006. The role of melt water in glacial processes. Sediment. Geol. 190, 257–268.

Ferguson, G., Beltrami, H., Woodbury, A.D., 2006. Perturbation of ground surface temperature reconstructions by groundwater flow? Geophys. Res. Lett. 33, L13708.

Ferris, F.G., Enright, A.M.L., Fortin, D., Clark, I.D., 2016. Rates of Fe(II)-oxidation and solubility of bacteriogenic iron oxides. Geomicrobiol. J. 33, 237–242.

Foster, S., Chilton, J., Nijsten, G.J., Richts, A., 2013. Groundwater – a global focus on the 'local resource'. Curr. Opin. Environ. Sustain. 5, 685–695.

Fu, C., James, A.L., Yao, H., 2014. SWAT-CS: revision and testing of SWAT for Canadian Shield catchments. J. Hydrol. 511, 719–735.

Gault, A.G., Ibrahim, A., Langley, S., Renaud, R., Takahashi, Y., Boothman, C., Lloyd, J.R., Clark, I.D., Ferris, F.G., Fortin, D., 2011. Microbial and geochemical features suggest iron redox cycling within bacteriogenic iron oxide-rich sediments. Chem. Geol. 281, 41–51.

Gault, A.G., Langley, S., Ibrahim, A., Renaud, R., Takahashi, Y., Boothman, C., Lloyd, J.R., Clark, I.D., Ferris, F.G., Fortin, D., 2012. Seasonal changes in mineralogy, geochemistry and microbial community of bacteriogenic iron oxides (BIOS) in a circumneutral wetland. Geomicrobiol. J. 29, 161–172.

Gleeson, T., Befus, K.M., Jasechko, S., Luijendijk, E., Cardenas, M.B., 2015. The global volume and distribution of modern groundwater. Nat. Geosci. 9, 161–169.

Goldscheider, N., Hunkeler, D., Rossi, P., 2006. Microbial biocenoses in pristine aquifers and an assessment of investigative methods. Hydrogeol. J. 14, 926–941.

Groffman, A.R., Crossey, L.J., 1999. Transient redox regimes in a shallow alluvial aquifer. Chem. Geol. 161, 415–442.

Glynn, P.D., Plummer, L.N., 2005. Geochemistry and the understanding of ground-water systems. Hydrogeol. J. 13, 263–287.

Jesußek, A., Grandel, S., Dahmke, A., 2013. Impacts of subsurface heat storage on aquifer hydrogeochemistry. Environ. Earth Sci. 69, 1999–2012.

Kato, S., Kikuchi, S., Kashiwabara, T., Takahashi, Y., Suzuki, K., Itoh, T., Ohkuma, M., Yamagishi, A., 2012. Prokaryotic abundance and community composition in a freshwater iron-rich microbial mat at circumneutral pH. Geomicrobiol. J. 29, 896–905.

Klein, C., Philpotts, A.R., 2013. Earth Materials: Introduction to Mineralogy and Petrology. Cambridge University Press, New York, USA.

Klueglein, N., Kappler, A., 2013. Abiotic oxidation of Fe(II) by reactive nitrogen species in cultures of the nitrate-reducing Fe(II) oxidizer Acidovorax sp. BoFeN1 – questioning the existence of enzymatic Fe(II) oxidation. Geobiology 11, 180–190.

Kumar, A.R., Riyazuddin, P., 2012. Seasonal variation of redox species and redox potentials in shallow groundwater: a comparison of measured and calculated redox potentials. J. Hydrol. 444, 187–198.

Kump, L.R., Brantley, S.R., Arthur, M.A., 2000. Chemical weathering, atmospheric CO2, and climate. Annu. Rev. Earth Planet. Sci. 28, 611–667.

Kurylyk, B.L., MacQuarrie, K.T.B., McKenzie, J.M., 2014. Climate change impacts on groundwater and soil temperatures in cold and temperate regions: implications, mathematical theory, and emerging simulation tools. Earth-Sci. Rev. 138, 313–334.

Langley, S., Gault, A.G., Ibrahim, A., Takahashi, Y., Renaud, R., Fortin, D., Clark, I.D., Ferris, F.G., 2009. A comparison of the rates of Fe(III) reduction in synthetic and bacteriogenic iron oxides by Shewanella putrefaciens CN32. Geomicrobiol. J. 26, 57–70.

Langmuir, D., 1997. Aqueous Environmental Geochemistry. Prentice Hall, New Jersey, USA.

Lewis, C.F.M., Karrow, P.F., Blasco, S.M., McCarthy, F.M.G., King, J.W., Moore, T.C., Rea, D.K., 2008. Evolution of lakes in the Huron basin: deglaciation to present. Aquat. Ecosyst. Health Manag. 11, 127–136.

Lin, D., Larsen, E.I., Larsen, G.R., Cox, M.E., Smith, J.E., 2012. Bacterially mediated iron cycling and associated biogeochemical processes in a subtropical shallow coastal aquifer: implications for groundwater quality. Hydrobiologia 696, 63–76.

McMahon, P.B., Chapelle, F.H., 2008. Redox processes and water quality of selected principal aquifer systems. Ground Water 46, 259–271.

Melton, E.D., Swanner, E.D., Behrens, S., Schmidt, C., Kappler, A., 2014. The interplay of microbially mediated and abiotic reactions in the biogeochemical Fe cycle. Nat. Rev. Microbiol. 12, 797–808.

Menberg, K., Blum, P., Kuryluk, B.L., Bayer, P., 2014. Observed groundwater temperature response to recent climate change. Hydrol. Earth Syst. Sci. 18, 4453–4466.

Mitchell, C.P.J., Branfireun, B.A., 2005. Hydrogeomorphic controls on reduction-oxidation conditions across Boreal upland-peatland interfaces. Ecosystems 8, 731–747.

Montcoudiol, N., Molson, J., Lemieux, J.M., 2015. Groundwater geochemistry of the Outaouais region (Quebec, Canada): a regional-scale study. Hydrogeol. J. 23, 377–396.

Parkhurst, D.L., Appelo, C.A.J., 2013. Description of Input and Examples for PHREEQC Version 3—A Computer Program for Speciation, Batch-reaction, One-dimensional Transport, and Inverse Geochemical Calculations: U.S. Geological Survey Techniques and Methods. book 6, chap. A43. U.S. Geological Survey, Denver, Colorado, U.S., p. 497

Parmar, N., Gorby, Y.A., Beveridge, T.J., Ferris, F.G., 2001. Formation of green rust and immobilization of nickel in response to bacterial reduction of hydrous ferric oxide. Geomicrobiol. J. 18, 375–385.

Parsons, C.T., Couture, R.M., Omoregie, E.O., Bardelli, F., Greneche, J.M., Roman-Ross, G., Charlet, L., 2013. The impact of oscillating redox conditions: arsenic

immobilization in contaminated calcareous floodplain soils. Environ. Pollut. 178, 254—263.

Richard, S.K., Chesnaux, R., Rouleau, A., Morin, R., Walter, J., Rafini, S., 2014. Field evidence of hydraulic connections between bedrock aquifers and overlying granular aquifer: examples from the Grenville Province of the Canadian Shield. Hydrogeol. J. 22, 1889—1904.

Roden, E.E., Sobolev, D., Glazer, B., Luther III, G.W., 2004. Potential for microscale bacterial Fe redox cycling at the aerobic-anaerobic interface. Geomicrobiol. J. 21, 379—391.

Shelobolina, E., Xu, H., Konishi, H., Kukkadapu, R., Wu, T., Blöthe, M., Roden, E., 2012. Microbial lithotrophic oxidation of structural Fe(II) in biotite. Appl. Environ. Microbiol. 78, 5746—5752.

Shen, Y., Chapelle, F.H., Strom, E.W., Benner, R., 2015. Origins and bioavailability of dissolved organic matter in groundwater. Biogeochemistry 122, 61—78.

Singer, S.N., Cheng, C.K., 2002. An Assessment of Groundwater Resources of Northern Ontario. Ministry of the Environment, Toronto, Ontario, Canada.

Shilts, W.W., Aylsworth, J.M., Kaszycki, C.A., Klassen, R.A., 1987. Canadian Shield. In: Graf, W.L. (Ed.), Geomorphic Systems of North America: Boulder Colorado, Geological Society of America, Centennial Special Volume, vol. 2, pp. 119—161.

Shirokova, V.L., Ferris, F.G., 2013. Microbial diversity and biogeochemistry of a shallow pristine Canadian Shield groundwater system. Geomicrobiol. J. 30, 1—10.

Taylor, C.A., Stefan, H.G., 2009. Shallow groundwater temperature response to climate change and urbanization. J. Hydrol. 375, 601—612.

Taylor, G.T., Scanlon, B., Döll, P., Rodell, M., van Beek, R., Wada, Y., Longuevergne, L., Leblanc, M., Famiglietti, J.S., Edmunds, M., Konikow, L., Green, T.R., Chen, J., Taniguchi, M., Bierkens, M.F.P., MacDonald, A., Fan, Y., Maxwell, R.M., Yechieli, Y., Gurdak, J.J., Allen, D.M., Shamsudduha, M., Hiscock, K., Yeh, P.J.F., Holman, I., Treidel, H., 2013. Ground water and climate change. Nat. Clim. Change 3, 322—329.

Ulanowski, T.A., Branfireun, B.A., 2013. Small-scale variability in peatland pore-water biogeochemistry, Hudson Bay Lowland, Canada. Sci. Total Environ. 454, 211—218.

Vienken, T., Dietrich, P., 2011. Field evaluation of methods for determining hydraulic conductivity from grain size data. J. Hydrol. 400, 58—71.

Vollrath, S., Behrends, T., Van Cappellen, P., 2012. Oxygen dependency of neutrophilic Fe(II) oxidation by *Leptothrix* differs from abiotic reaction. Geomicrobiol. J. 29, 550—560.

Vollrath, S., Behrends, T., Koch, C.B., Van Cappellen, P., 2013. Effects of temperature on rates and mineral products of microbial Fe(II) oxidation by *Leptothrix cholodnii* at microaerobic conditions. Geochim. Cosmochim. Acta 108, 107—124.

Wilson, M.J., 2004. Weathering of the primary rock-forming minerals: processes, products, and rates. Clay Miner. 39, 233—266.

Zhu, K., Bayer, P., Grathwohl, P., Blum, P., 2015. Groundwater temperature evolution in the subsurface urban heat island of Cologne, Germany. Hydrol. Process. 29, 965—978.